

Response to editor comments

Comments to the Author:

Dear Dr. Lavergne,

Thank you for submitting a revised version of your manuscript "Modelling tree-ring cellulose $\delta^{18}\text{O}$ variations of two temperature-sensitive tree species from North and South America". Please find a few additional minor suggestions and typos to correct. I also invite you to have another careful read of your manuscript, including figure legends and references.

Best regards,

Laurie Menviel

AC : We thanks the Editor for her additional suggestions in the text.

L. 44: "is more likely linked to the" do you want to say "is primarily linked to"?

AC : Yes. We have changed this part of the sentence as suggested by the Editor.

Move L. 133-134 (location of the model) to a new section "Code and data availability" to be added at the end of manuscript (right before the acknowledgment section).

Move L. 165-166 (IAEA web address) to the new section "Code and data availability"

Move L. 181-182: "extracted at <http://paos.colorado.edu/~dcn/SWING/database.php>" to the new section "Code and data availability"

Move L. 209: "provided by the NOAA/OAR/ESRL (https://www.esrl.noaa.gov/psd/data/gridded/data.20thC_ReanV2c.html)," to the new section "Code and data availability"

Move L. 220: " <http://cfs.nrcan.gc.ca/projects/3/4>" to the new section "Code and data availability"

AC : We have added a 'Code and data availability' section before the Acknowledgement one as suggested by the Editor. We have moved in this new section all the references to each datasets used.

Please modify as follow:

L. 180: "(1) The Melbourne University model (MUGCM)"

L. 183: "the Laboratoire de Météorologie Dynamique Zoom model (LMDZ5A)"

Please rephrase: L. 227 “as displayed in the observations” or “as shown”

L. 324: Please rephrase “are more highly correlated” as I don’t think it is grammatically correct. Some suggestions: “are highly correlated” or “have a higher correlation coefficient”

Reviewer 1 suggested to use “tree rings” please use this spelling throughout the manuscript (i.e. change all the “tree-rings”, e.g. title, section 2.1, legend of figure 1, keywords...).

L. 476: “we have provided”

L. 733: please add a space between “ones” and “with” or rephrase: “The tests sites from Quebec are in black and the Argentinean ones are in red.”

Legend of figure 3: Please spell out “DOY”

AC : We have changed all the parts mentioned above as suggested by the Editor.

Legend of figure 4: “densities of probability of the coefficient of correlation” should it be instead “probability density functions”?

AC : We have changed ‘densities of probability’ into ‘density distributions’ in the legend of Figure 4, as done in Figure 5.

Figure 4 and 5: As already noted by Reviewer 1 the y axis should be “Kernel” and not “Kernal”, please correct. Also in figure 5 the y axis should read “Kernel density estimate”

AC : We have corrected ‘Kernal’ into ‘Kernel’ in Figures 4 and 5, and the y axis legend of Figures 5 and SM3.

Modelling tree ring cellulose $\delta^{18}\text{O}$ variations of two temperature-sensitive tree species from North and South America

Authors:

Aliénor Lavergne¹, Fabio Gennaretti¹, Camille Risi², Valérie Daux³, Etienne Boucher⁴, Martine M. Savard⁵, Maud Naulier⁶, Ricardo Villalba⁷, Christian Bégin⁵ and Joël Guiot¹

¹Aix Marseille Université, CNRS, IRD, Collège de France, CEREGE, ECCOREV, Aix-en-Provence, France

²Laboratoire de Météorologie Dynamique, IPSL, UPMC, CNRS, Paris, France

³Laboratoire des Sciences du Climat et de l'Environnement, CEA-CNRS-UVSQ, 91191 Gif-sur-Yvette, France

⁴Department of Geography and GEOTOP, Université du Québec à Montréal, Montréal, Canada

⁵Geological Survey of Canada, Natural Resources Canada, 490 rue de la Couronne, QC, G1K9A9, Canada

⁶Institut de Radioprotection et de Sûreté Nucléaire (IRSN), PRP-ENV, SERIS/LRTE, Saint-Paul-lez-Durance, France

⁷Instituto Argentino de Nivología, Glaciología y Ciencias Ambientales, IANIGLA-CONICET, Mendoza, Argentina

Corresponding authors: Aliénor Lavergne (alienor.lavergne@gmail.com) and Fabio Gennaretti (gennaretti@cerege.fr)

Tel : +33 (0) 4 42 97 15 32

Centre Européen de Recherche et d'Enseignement en Géosciences

Technopôle de l'Arbois-Méditerranée

13545 Aix-en-Provence, FRANCE

Aliénor Lavergne 9/10/y 14:14

Définition du style: Police par défaut

Aliénor Lavergne 9/10/y 14:14

Supprimé: -

30 **ABSTRACT**

31 Oxygen isotopes in tree rings ($\delta^{18}\text{O}_{\text{TR}}$) are widely used to reconstruct past climates. However, the
32 complexity of climatic and biological processes controlling isotopic fractionation is not yet fully
33 understood. Here, we use the MAIDENiso model to decipher the variability of $\delta^{18}\text{O}_{\text{TR}}$ of two
34 temperature-sensitive species of relevant paleoclimatological interest (*Picea mariana* and
35 *Nothofagus pumilio*) and growing at cold high-latitudes in North and South America. In this first
36 modelling study on $\delta^{18}\text{O}_{\text{TR}}$ values in both northeastern Canada (53.86°N) and western Argentina
37 (41.10°S), we specifically aim at: 1) evaluating the predictive skill of MAIDENiso to simulate
38 $\delta^{18}\text{O}_{\text{TR}}$ values, 2) identifying the physical processes controlling $\delta^{18}\text{O}_{\text{TR}}$ by mechanistic modelling
39 and, 3) defining the origin of the temperature signal recorded in the two species. Although the
40 linear regression models used here to predict daily $\delta^{18}\text{O}$ of precipitation ($\delta^{18}\text{O}_{\text{P}}$) may need to be
41 improved in the future, the resulting daily $\delta^{18}\text{O}_{\text{P}}$ values adequately reproduce observed (from
42 weather stations) and simulated (by global circulation model) $\delta^{18}\text{O}_{\text{P}}$ series. The $\delta^{18}\text{O}_{\text{TR}}$ values of
43 the two species are correctly simulated using the $\delta^{18}\text{O}_{\text{P}}$ estimation as MAIDENiso input, although
44 some offset in mean $\delta^{18}\text{O}_{\text{TR}}$ levels is observed for the South American site. For both species, the
45 variability of $\delta^{18}\text{O}_{\text{TR}}$ series is **primarily** linked to the effect of temperature on isotopic enrichment
46 of the leaf water. We show that MAIDENiso is a powerful tool for investigating isotopic
47 fractionation processes but that the lack of a denser isotope-enabled monitoring network
48 recording oxygen fractionation in the soil-vegetation-atmosphere compartments limits our
49 capacity to decipher the processes at play. This study proves that the eco-physiological modelling
50 of $\delta^{18}\text{O}_{\text{TR}}$ values is necessary to interpret the recorded climate signal more reliably.

51

52 **Keywords:** MAIDENiso model, $\delta^{18}\text{O}$, tree ring, *Nothofagus pumilio*, *Picea mariana*

53

54

55

Aliénor Lavergne 9/10/y 14:14

Supprimé: more likely

Aliénor Lavergne 9/10/y 14:14

Supprimé: rather than on the isotopic composition of the source water.

Aliénor Lavergne 9/10/y 14:14

Supprimé: -

60 1. INTRODUCTION

61 Oxygen isotopes in tree rings ($\delta^{18}\text{O}_{\text{TR}}$) are increasingly used as indicators of past climatic
62 changes in temperate areas (Cernusak and English, 2015; Hartl-Meier et al., 2014; Saurer et al.,
63 2008). They have been widely used to reconstruct past atmospheric conditions such as air
64 temperature (Naulier et al., 2015), drought (Labuhn et al., 2016), precipitation amount (Rinne et
65 al., 2013), isotopic composition of precipitation (Danis et al., 2006), relative air humidity
66 (Wernicke et al., 2015), cloud cover (Shi et al., 2012), and even atmospheric circulation patterns
67 (Brienen et al., 2012). This diversity of climatic targets possibly reconstructed based on oxygen
68 isotopes hints at the challenge of understanding the complexity of the climatic and biological
69 processes that control isotopic fractionation of oxygen in trees (Treydte et al., 2014).
70 Uncertainties arise because different poorly measured factors influence $\delta^{18}\text{O}_{\text{TR}}$ values. Isotopic
71 signals in tree rings cellulose are strongly influenced by isotopic signature of soil water taken up
72 by the roots and by evaporative and physiological processes occurring at the leaf level and during
73 downstream metabolism (Barbour et al., 2005; Gessler et al., 2014). Thus, a comprehensive
74 approach that embraces existing mechanistic understanding of the fractionation processes
75 involved is required.

76
77 Few isotopic process-based models have been developed to investigate the mechanistic rules
78 governing the $\delta^{18}\text{O}_{\text{TR}}$ variations (Guiot et al., 2014): the Péclet-modified Craig-Gordon model
79 (Kahmen et al., 2011) and the Roden's model (Roden et al., 2000) are able to estimate, at a daily
80 time step, the $\delta^{18}\text{O}$ values of soil and xylem waters, and the isotopic fractionation occurring in the
81 leaves due to evapotranspiration. Versions of these models are integrated in more complete forest
82 ecophysiological models simulating the ensemble of forest water and carbon fluxes: (1)
83 MAIDEN (Modeling and Analysis In DENdroecology) (Gea-Izquierdo et al., 2015; Misson,
84 2004), which contains the isotopic module MAIDENiso (Danis et al., 2012) and (2) MUSICA
85 (Ogée et al., 2003, 2009). Both are accounting for important post-photosynthetic factors and are
86 able to link photosynthesis and carbohydrate allocation to stem growth.

87
88 In this paper, we use the MAIDENiso model to decipher the $\delta^{18}\text{O}_{\text{TR}}$ variability in American
89 temperature-sensitive species (*Picea mariana* in northeastern Canada and *Nothofagus pumilio* in
90 western Argentina). The selected sites are of special interest for paleoclimatology given that their

Aliénor Lavergne 9/10/y 14:14
Supprimé: -

92 $\delta^{18}\text{O}_{\text{TR}}$ chronologies carry strong temperature signals. A summer temperature reconstruction was
93 already developed at the North American site (Gennaretti et al., 2017b; Naulier et al., 2015) and a
94 calibration study conducted at the South American one highlighted the strong potential of $\delta^{18}\text{O}_{\text{TR}}$
95 values to reflect variations in summer-autumn temperatures over a large region south of 38°S
96 (Lavergne et al., 2016). However, up to now, the climate- $\delta^{18}\text{O}_{\text{TR}}$ relationships were analysed
97 using a black box approach based on linear models. Here, we specifically aim at: 1) evaluating
98 the predictive skill of MAIDENiso to simulate $\delta^{18}\text{O}_{\text{TR}}$ values, 2) identifying the physical
99 processes controlling $\delta^{18}\text{O}_{\text{TR}}$ by mechanistic modelling and, 3) defining the origin of the
100 temperature signal recorded in the two species.

101

102 2. DATA AND METHODS

103 2.1. Sampling sites and tree-ring data

104 Two high-latitude American native species were studied here: 1) *Picea mariana* (Mill. B.S.P.;
105 black spruce), which is a conifer widely distributed over the American boreal forest (Viereck and
106 Johnston, 1990); and 2) *Nothofagus pumilio* (Poepp. et Endl. Krasser; lenga), which is an
107 angiosperm deciduous species dominating the high-elevation forests along the Patagonian Andes
108 from 35°S to 55°S (Donoso, 1981; Schlatter, 1994). We selected two sites of *P. mariana* in the
109 centre of the Quebec-Labrador Peninsula in northeastern Canada (L01 and L20; from 53°51'N-
110 72°24'W to 54°33'N-71°14'W, ~480 m elevation; see Gennaretti et al. (2014) and Naulier et al.
111 (2014) for details) and three sites of *N. pumilio* in northern Patagonia, western Argentina (NUB,
112 ALM and CHA; from 41°09'S-71°48'W to 41°15'S-71°17'W, 1270-1610 m elevation; see
113 Lavergne et al. (2016, 2017) for details). Climate in northeastern Canada is mostly continental
114 and subarctic with short, mild and wet summers and long, cold and dry winter. Total annual
115 precipitation averages 825 mm with up to 46% falling during the growing season in summer
116 (June to September) (Naulier et al., 2014). In western Argentina, precipitation is largely
117 concentrated from late fall to early spring (May-November) followed by a drier and mild period
118 during summer and early fall (December-April) (López Bernal et al., 2012).

119

120 Four trees per site were collected for both species. The selection of the samples and analytical
121 procedure for $\delta^{18}\text{O}_{\text{TR}}$ measurements were described in Lavergne et al. (2016) and Naulier et al.

122 (2014). The developed $\delta^{18}\text{O}_{\text{TR}}$ chronologies covered the 1950-2005 and 1952-2011 periods at the
123 northeastern Canadian and western Argentinian sites, respectively. The chronologies that were
124 built for each species were significantly correlated between stands (Figure 1). This supported the
125 construction of a combined isotope chronology for both the northeastern Canada and western
126 Argentina sites.

127 2.2. Modelling oxygen isotopes in tree ring cellulose with MAIDENiso

129 MAIDENiso is a process-based model that can simulate in parallel phenological and
130 meteorological controls on photosynthetic activity and carbon allocation (Danis et al., 2012). It
131 explicitly allocates carbohydrates to different carbon pools (leaves, stem, storage and roots) on a
132 daily basis using phenological stage-dependent rules (see Gennaretti et al. (2017b) for details on
133 the construction of the main MAIDEN model). It also simulates the fractionation of carbon and
134 oxygen isotopes during growth processes. In particular, it estimates at a daily time step $\delta^{18}\text{O}$
135 values of soil water and xylem water, the isotopic fractionation occurring in the leaves due to
136 evapotranspiration and the biochemical fractionation during cellulose formation. It uses as input
137 daily maximum and minimum temperature ($^{\circ}\text{C}$), precipitation (cm/day), atmospheric CO_2
138 concentration (ppm) and $\delta^{18}\text{O}$ values of precipitation ($\delta^{18}\text{O}_{\text{P}}$ in ‰).

140 In this study, the calculation of the daily $\delta^{18}\text{O}_{\text{TR}}$ in tree ring cellulose (‰) is based on the (Danis
141 et al., 2012)'s formulation of the Craig-Gordon model (Craig and Gordon, 1965):

$$142 \quad \delta^{18}\text{O}_{\text{TR}} = (1-f_o) \cdot [\epsilon^* + \epsilon_k \cdot (1-h_{\text{air}}) + h_{\text{air}} \cdot \delta^{18}\text{O}_{\text{V}} + (1-h_{\text{air}}) \cdot \delta^{18}\text{O}_{\text{XW}}] + f_o \cdot \delta^{18}\text{O}_{\text{XW}} + \epsilon_0 \quad (1)$$

143 This equation summarizes how $\delta^{18}\text{O}_{\text{TR}}$ is determined by:

144 (i) the $\delta^{18}\text{O}$ of the source (xylem) water ($\delta^{18}\text{O}_{\text{XW}}$), which is computed by averaging the
145 $\delta^{18}\text{O}_{\text{SW}}$ values of the different soil layers weighted by the volume of water taken up by
146 the roots in each layer. The isotopic effects of water mixing and soil evaporation on
147 the $\delta^{18}\text{O}_{\text{SW}}$ values of the different soil layers are computed by a mass and isotopic
148 balance (Danis et al., 2012). It is worth noting that no fractionation occurs during
149 water uptake by roots (Wershaw et al., 1966), neither during the transport of water
150 from the roots to the leaves.

151 (ii) the ^{18}O enrichment of the leaf water due to transpiration is described by
152 $(\epsilon^* + \epsilon_k \cdot (1-h_{\text{air}}) + h_{\text{air}} \cdot \delta^{18}\text{O}_{\text{V}} + (1-h_{\text{air}}) \cdot \delta^{18}\text{O}_{\text{XW}})$ after Craig and Gordon (1965), where:

Aliénor Lavergne 9/10/y 14:14

Supprimé: -

Aliénor Lavergne 9/10/y 14:14

Supprimé: The code of the model can be found
here:
<https://doi.org/10.6084/m9.figshare.5446435.v1>.

Aliénor Lavergne 9/10/y 14:14

Supprimé: -

Aliénor Lavergne 9/10/y 14:14

Supprimé: (

Aliénor Lavergne 9/10/y 14:14

Supprimé: ,

- a. ϵ^* is the equilibrium fractionation due to the change of phase from liquid water to vapour at the leaf temperature (fixed at 21.4°C, the temperature threshold for maximum carbon assimilation, ϵ^* is 9.65‰ (Helliker and Richter, 2008)),
 - b. ϵ_k is the kinetic fractionation due to the diffusion of vapour into unsaturated air through the stomata and the leaf boundary layer,
 - c. h_{air} is the relative humidity of the evaporating air mass estimated from daily air temperature (T_{air} , °C; mean of the maximum and minimum air temperatures), and the dew point temperature (T_r , °C) (Running et al., 1987),
 - d. $\delta^{18}O_V$ is the atmospheric water vapour calculated assuming a precipitation-vapour isotopic equilibrium (see below);
- (iii) the biochemical fractionations (ϵ_0) due to oxygen exchange between carbonyl groups (C = O) in the organic molecules and water (DeNiro and Epstein, 1979; Farquhar et al., 1998).
 - (iv) the dampening factor f_o reflecting the exchange of the oxygen atoms between sucrose and xylem water during cellulose synthesis in the xylem cells of tree rings.

As previously evoked (i), $\delta^{18}O_{XW}$ of Eq. 1 depends on $\delta^{18}O_{SW}$ and thus on $\delta^{18}O_P$ values. However, long continuous time series of $\delta^{18}O_P$ are not available in the studied area. Here, we tested the impact of using two different methods for deriving $\delta^{18}O_P$ time series.

First, a linear model was used to estimate the daily values of $\delta^{18}O_P$ and subsequently $\delta^{18}O_V$ based on the primary drivers of their temporal variability (Dansgaard, 1964; Horita and Wesolowski, 1994), that are air temperature (T_{air} , °C) and precipitation at the corresponding site (P ; mm):

$$\delta^{18}O_P = a \cdot T_{air} + b \cdot P + c \quad (2)$$

$$\delta^{18}O_V = \delta^{18}O_P - \epsilon^*_{T_{air}} \quad (3)$$

with $\epsilon^*_{T_{air}}$ the fractionation due to the change of phase from liquid water to vapour at the mean air temperature. The coefficients a and b were allowed to vary over a plausible range (or prior range) in the calibration process together with other MAIDENiso parameters, while coefficient c was fixed to a likely value (see Table 1 and section 2.4). This estimated set of data is referred in the following as the estimated $\delta^{18}O_P$ dataset.

Second, we run the model with the series of the daily $\delta^{18}O_P$ derived from two general circulation models (GCM) with different spatial resolutions and enough available data at our site locations:

Aliénor Lavergne 9/10/y 14:14
Supprimé: (see http://www-naweb.iaea.org/naweb/ih/IHS_resources_gnip.html).

1) the [Melbourne University](#) model ([MUGCM](#); Noone and Simmonds, 2002) forced by varying sea surface temperature (SST) from the HadISST data set for the 1950-2003 period ($2^\circ \times 2^\circ$ resolution; hereafter referred as MUGCM $\delta^{18}\text{O}_\text{P}$ dataset), and 2) the Laboratoire de Météorologie Dynamique Zoom model (LMDZ5A; Hourdin et al. (2013); Risi et al. (2010)) with the horizontal winds guided by those of the National Centers for Environmental Protection - 20th Century Reanalysis (NCEP20) for the 1950-2008 period (Compo et al., 2011) ($2.5^\circ \times 3.75^\circ$ resolution; hereafter referred as LMDZ-NCEP20 $\delta^{18}\text{O}_\text{P}$ dataset).

The final $\delta^{18}\text{O}_\text{TR}$ time series are the annual average of the $\delta^{18}\text{O}_\text{TR}$ daily values (Eq. 1) weighted by the daily simulated stand Gross Primary Production (GPP), assuming a proportional allocation of carbon to the trunk. For the northeastern Canadian sites, the GPP simulated by MAIDENiso was optimized using observations from an eddy covariance station (see Gennaretti et al. (2017a)). Unfortunately, such observations were not available for *N. pumilio*, and therefore the parameterization obtained for the GPP of *P. mariana* was also used for the western Argentinian sites but constraining the simulations with phenological observations extracted from the literature. For example, to respect the annual cycle of the leaf area index (LAI) for *N. pumilio* (Magnin et al., 2014; Rusch, 1993), we used in MAIDENiso a seasonal LAI annual cycle with a development of leaves (LAI increase) between October and November, a maximum LAI (set at 5 leaf area/ground area) from November to April, a decreasing LAI (leaf fall) between April and May, and finally a leafless period (null LAI) from June to September (Magnin et al., 2014; Rusch, 1993). Furthermore, based on the finding that $\delta^{18}\text{O}_\text{TR}$ annual time series were more correlated to climate variables of specific months of the growing season (Lavergne et al., 2016), we also computed $\delta^{18}\text{O}_\text{TR}$ annual values by weighting the $\delta^{18}\text{O}_\text{TR}$ daily values (Eq. 1) with synthetic GPP time series maximizing the correspondence between observations and simulations.

2.3. Meteorological and atmospheric CO₂ data

At the western Argentinian sites, we did not have long daily records of observed climate data. Therefore, daily minimum–maximum temperature and precipitation data were derived from the 20th Century Reanalysis V2c ($2^\circ \times 2^\circ$ resolution; Compo et al., 2011), which is one of the few reanalysis products covering entirely the 20th century. The temperature daily time series of the reanalysis were corrected in order to respect the monthly mean values detected at Bariloche, the

Aliénor Lavergne 9/10/y 14:14

Supprimé: MUGCM

Aliénor Lavergne 9/10/y 14:14

Supprimé: (

Aliénor Lavergne 9/10/y 14:14

Supprimé: extracted at
<http://paos.colorado.edu/~dcn/SWING/database.php>;

Aliénor Lavergne 9/10/y 14:14

Supprimé:) model

Aliénor Lavergne 9/10/y 14:14

Supprimé: (

Aliénor Lavergne 9/10/y 14:14

Supprimé: ..

Aliénor Lavergne 9/10/y 14:14

Supprimé: :

Aliénor Lavergne 9/10/y 14:14

Supprimé: ..

Aliénor Lavergne 9/10/y 14:14

Supprimé:)

Aliénor Lavergne 9/10/y 14:14

Supprimé: (

Aliénor Lavergne 9/10/y 14:14

Supprimé: provided by the NOAA/OAR/ESRL
($2^\circ \times 2^\circ$ resolution,
https://www.esrl.noaa.gov/psd/data/gridded/data.20thC_ReanV2c.html),

238 nearest meteorological station from our sampling sites (~48 km from the sites, 41°12' S–71°12'
 239 W, 840 m asl; Servicio Meteorológico Nacional, Argentina). The resulting maximum and
 240 minimum temperature series, covering the 1952–2011 period, fit well with the daily local
 241 temperature data from La Almohadilla (ALM) site (41°11'S, 71°47'W, 1410 m asl; data
 242 measured by dataloggers and provided by IANIGLA) available over the 2002–2012 period ($r =$
 243 0.74, $p < 0.001$; Figure SM1). For the northeastern Canadian sites, climate data were obtained
 244 from the gridded interpolated Canadian database of daily minimum–maximum temperature and
 245 precipitation covering the 1950–2005 studied period (0.08°×0.08° resolution; Hutchinson et al.,
 246 2009). In addition to these data we also used modelled daily data from the GCMs described
 247 above for both the western Argentinian and northeastern Canadian sites (see Table 2 with the
 248 input data used for each tested configuration).

250 Data on the atmospheric CO₂ concentration were derived from the Mauna Loa station over the
 251 1958–2012 period (Keeling et al., 1976). For the years 1950–1957, we extrapolated atmospheric
 252 CO₂ data using the trend and seasonal cycle **as displayed** in the observations over the subsequent
 253 10-years period (1958–1967).

254 2.4. Estimation of parameters influencing $\delta^{18}\text{O}_{\text{TR}}$

256 We used a Bayesian method for the simultaneous calibration of the various MAIDENiso
 257 parameters specific to the study species and site. A set of 50 plausible blocks of parameters
 258 (posterior values) was selected according to the method described in Gennaretti et al. (2017a)
 259 using Markov Chain Monte Carlo (MCMC) sampling (Table 1). The following prior plausible
 260 ranges were considered:

261 1) the prior ranges of the a and b coefficients in the equation of the daily $\delta^{18}\text{O}_p$ (Eq. 2) were
 262 selected in order to get $\delta^{18}\text{O}_p$ values for each site consistent with the measured monthly local
 263 values from the nearest stations of the Global Network of Isotopes in Precipitation (GNIP), and
 264 with the simulated daily values from the LMDZ–NCEP20 model and from the MUGCM model
 265 (see Table 1),

266 2) the range for the biochemical fractionation factor ϵ_0 was chosen between 24‰ and 30‰
 267 (+27±3‰ after DeNiro and Epstein (1981), Sternberg (1989) and Yakir and DeNiro (1990)),

Aliénor Lavergne 9/10/y 14:14

Supprimé: ;

Aliénor Lavergne 9/10/y 14:14

Supprimé: (

Aliénor Lavergne 9/10/y 14:14

Supprimé: ; <http://cfs.nrcan.gc.ca/projects/3/4>).

Aliénor Lavergne 9/10/y 14:14

Supprimé: . (

Aliénor Lavergne 9/10/y 14:14

Supprimé: ;
<http://www.esrl.noaa.gov/gmd/ccgg/trends/>).

Aliénor Lavergne 9/10/y 14:14

Supprimé: observed

Aliénor Lavergne 9/10/y 14:14

Supprimé:);

Aliénor Lavergne 9/10/y 14:14

Supprimé:);

277 3) the range for the kinetic fractionation ϵ_k , which has been set to 26.5‰ in Farquhar et al. (1989)
278 but that can vary over larger ranges (Buhay et al., 1996), was taken between 10‰ and 30‰ here,
279 4) the range for the dampening factor f_o was allowed to vary between 0.3 and 0.5 following
280 Saurer et al. (1997).

281
282 We tested the sensitivity of the MAIDENiso model to the calibrated parameters by modifying
283 them within their respective prior calibration range. To control the robustness of the calibrated
284 parameters, we performed the calibration of these parameters over two equal length intervals
285 (1950-1977 and 1978-2005 for *P. mariana*; 1952-1981 and 1982-2011 for *N. pumilio*) keeping
286 the second half for independent validation of the parameters estimates. Once the model was
287 calibrated for the two species, the MAIDENiso's performance to simulate *P. mariana* and *N.*
288 *pumilio* $\delta^{18}\text{O}_{\text{TR}}$ interannual data was evaluated using the correlation coefficients (r) and the root
289 mean square errors (RMSE) between observed and simulated values. This is a standard approach
290 to evaluate how well a mechanistic model is simulating $\delta^{18}\text{O}_{\text{TR}}$ variations (e.g. Danis et al., 2012;
291 Lorrey et al., 2016).

292 293 **2.5. Disentangling leaf-level fractionation processes and source water influences on** 294 **$\delta^{18}\text{O}_{\text{TR}}$ signature**

295 To define the relative contributions to the $\delta^{18}\text{O}_{\text{TR}}$ signature of the isotopic signal of the source
296 water (xylem water) and of the fractionation processes due to transpiration taking place in the
297 leaves, we designed two experimental simulations with MAIDENiso based on Eq. 1:

- 298 1) to quantify the influence of the variability of the isotopic composition of the xylem water
299 on $\delta^{18}\text{O}_{\text{TR}}$, we compared the reference simulations to those where the relative humidity
300 (h_{air}) and the isotopic composition of atmospheric vapour ($\delta^{18}\text{O}_{\text{V}}$) were assumed to be
301 constant. The constant values for h_{air} and $\delta^{18}\text{O}_{\text{V}}$ were defined as the averages of the
302 respective MAIDENiso outputs ($h_{\text{air}} = 0.62$ and 0.9 , and, $\delta^{18}\text{O}_{\text{V}} = -26.28\text{‰}$ and -17.34‰ ,
303 respectively for northeastern Canada and western Argentina; the XW source experiment
304 simulation hereafter),
- 305 2) to quantify the influence of the isotopic enrichment of the leaf water due to transpiration
306 on $\delta^{18}\text{O}_{\text{TR}}$, we compared the reference simulations to those where the $\delta^{18}\text{O}_{\text{XW}}$ series were
307 assumed to be constant. The constant value for $\delta^{18}\text{O}_{\text{XW}}$ was estimated as the average of

Aliénor Lavergne 9/10/y 14:14
Supprimé: .

the $\delta^{18}\text{O}_{\text{XW}}$ MAIDENiso outputs ($\delta^{18}\text{O}_{\text{XW}} = -13.81\text{‰}$ and -7.03‰ , respectively for northeastern Canada and western Argentina; the Leaf water enrichment driven experiment simulation hereafter).

Comparison between the experimental and reference simulations (i.e. using the optimal values of the parameters) was achieved through the calculation of the coefficient of determination (R^2).

3. RESULTS

3.1. Estimated versus modelled and observed $\delta^{18}\text{O}_\text{P}$ values

The modelled $\delta^{18}\text{O}_\text{P}$ series from the GCM models are similar to the GNIP datasets, with mean values ranging from -12‰ to -8‰ over June-September in northeastern Canada (Figure SM2A) and from -7‰ to -3‰ over December-April at the western Argentinian sites (Figure SM2B). In general, $\delta^{18}\text{O}_\text{P}$ series from LMDZ-NCEP20 model in western Argentina are slightly displaced toward higher values ($+1\text{‰}$) in comparison with the GNIP and MUGCM data. The estimated $\delta^{18}\text{O}_\text{P}$ values based on plausible values of coefficients a and b agree well with those of the models and observations in northeastern Canada. For the western Argentinian sites, they are 2-3‰ lower from April to October, i.e. late spring-early autumn (Figure SM2).

3.2. Sensitivity of the model to the calibrated parameters

Most of the calibrated parameters have an influence on the correlations between observed and simulated $\delta^{18}\text{O}_{\text{TR}}$ series and/or on the mean levels of the simulated series (Figure 2). The temperature and precipitation dependences of $\delta^{18}\text{O}_\text{P}$ values (respectively a and b coefficients) have the strongest influence on correlations. Increasing a and b values increase the mean $\delta^{18}\text{O}_{\text{TR}}$ levels, more strongly in western Argentina than in northeastern Canada (Figure 2). Changes in the dampening factor (f_o) and in the biochemical fractionation (ϵ_o) have almost no effect on correlation, but their increase induces significant decrease of the mean levels of $\delta^{18}\text{O}_{\text{TR}}$ series. Finally, increasing the kinetic fractionation (ϵ_k) leads to lower correlations and to higher mean levels of $\delta^{18}\text{O}_{\text{TR}}$ (Figure 2).

3.3. MAIDENiso performance in reproducing observed $\delta^{18}\text{O}_{\text{TR}}$ series

Split-period verifications of the calibrated relationships for *P. mariana* and *N. pumilio* when using estimated $\delta^{18}\text{O}_\text{P}$ series from Eq. 2 indicate that the calibration over either the first half or the

second half periods provide similar posterior densities of the calibrated parameters than the ones obtained when calibrating over the whole periods (Figure SM3). One exception is observed in the calibration of coefficient a in northeastern Canada over the two half periods, where the posterior densities of a are different from the one obtained by calibrating over the entire period. Over the entire periods, observed and simulated $\delta^{18}\text{O}_{\text{TR}}$ series are significantly correlated in northeastern Canada ($r = 0.56$, $p < 0.01$ and $\text{RMSE} = 0.67$; Figure 3A) and in western Argentina ($r = 0.48$, $p < 0.01$ and $\text{RMSE} = 0.63$; Figure 3C). The correlation between observed and simulated $\delta^{18}\text{O}_{\text{TR}}$ series are slightly improved when we used synthetic daily GPP ($r = 0.62$ and $r = 0.52$, $p < 0.01$, respectively for northeastern Canada and western Argentina; Figure 3B and 3D). It is worth noting that the mean levels of the simulated $\delta^{18}\text{O}_{\text{TR}}$ series for the Argentinian sites are lower than those of the observations (offset of around -2.5‰ ; Figure SM4). The series were therefore corrected to respect the mean values detected in the observations (Figure 3C and 3D). In contrast, the correlations between observation and simulation considerably decrease when we used modelled $\delta^{18}\text{O}_{\text{P}}$ from MUGCM models or LMDZ-NCEP20 reanalysis data. They only reach $r = 0.13$ ($p > 0.05$) to 0.23 ($p < 0.05$) in northeastern Canada and $r = 0.23$ to 0.26 ($p < 0.05$) in western Argentina, respectively (Figure 4).

3.4. Influence of source water and leaf water isotopic enrichment to the $\delta^{18}\text{O}_{\text{TR}}$ signature

The relative contributions to the $\delta^{18}\text{O}_{\text{TR}}$ signature of the isotopic signal of the source (xylem) water and of the ^{18}O enrichment of the leaf water due to transpiration were investigated. In both regions, the Leaf water enrichment experimental simulations and the reference simulations have a higher correlation coefficient (R^2 centred on 0.9 and 0.95, respectively for northeastern Canada and western Argentina; Figure 5) than are the XW source simulations with the reference simulations (R^2 centred on 0.65 and 0.8, respectively for northeastern Canada and western Argentina). This suggests that, with the model, the variability of $\delta^{18}\text{O}_{\text{XW}}$ has a weaker influence on $\delta^{18}\text{O}_{\text{TR}}$ variations than the changes of the leaf water isotopic enrichment do. Notably, *P. mariana* in northeastern Canada appears to be more sensitive to both influences than *N. pumilio* in western Argentina (Figure 5).

4. DISCUSSION

4.1. Precipitation $\delta^{18}\text{O}_{\text{P}}$ variations and estimation

Aliénor Lavergne 9/10/y 14:14
Supprimé: are more highly related to

372 Although the regression models used to predict daily $\delta^{18}\text{O}_\text{P}$ values are likely too simplistic, the
373 resultant monthly averaged values adequately reproduce the distribution of the observed (from
374 GNIP stations) and modelled (by GCMs) monthly $\delta^{18}\text{O}_\text{P}$ series in northeastern Canada. In
375 western Argentina, the distribution of monthly $\delta^{18}\text{O}_\text{P}$ values is also well reproduced but the
376 amplitude of variation of the predicted values is too high, leading to simulated values lower than
377 the measured ones during the colder months. The temporal $\delta^{18}\text{O}_\text{P}$ variations are positively related
378 to air temperature given the positive coefficient a . In agreement with the simple Rayleigh
379 distillation model (Dansgaard, 1964), as air temperature decreases, the specific humidity at
380 saturation decreases, and water vapour condenses. H_2^{18}O condenses preferentially, the residual
381 water vapour gets more and more depleted as condensation proceeds. Consequently, in the
382 Tropics, the $^{18}\text{O}/^{16}\text{O}$ ratio in the meteoric water has been observed to decrease with increasing
383 amount of precipitation and/or relative humidity (Rozanski et al., 1993). In extra-tropical regions,
384 $\delta^{18}\text{O}_\text{P}$ may also correlate with precipitation amount (negative coefficient b), since both variables
385 depend on the meteorological conditions.

386 The results of the linear regressions show comparatively lower influence of precipitation on
387 $\delta^{18}\text{O}_\text{P}$ in western Argentina than in northeastern Canada (Table 1). This suggests that the imprint
388 of the precipitation amount on $\delta^{18}\text{O}_\text{P}$ in western Argentina is low and that $\delta^{18}\text{O}_\text{P}$ variations are
389 mainly controlled by seasonal changes in temperature, which is in agreement with previous work
390 (Rozanski et al., 1995). However, due to the strong west-to-east precipitation gradient in this
391 region (orographic rain shadow), large $\delta^{18}\text{O}_\text{P}$ variations occur over short distances (Rozanski et
392 al., 1995; Smith and Evans, 2007; Stern and Blisniuk, 2002). Therefore, the daily precipitation
393 dataset extracted from the gridded reanalysis data, which has a low spatial resolution (>200 km),
394 may not represent the daily variations in precipitation at a local scale faithfully. Therefore, the
395 model may underestimate the contribution of precipitation on $\delta^{18}\text{O}_\text{P}$ variability in this particular
396 area.

397
398 In contrast, in northeast Canada, both temperature and precipitation amount equally control the
399 $\delta^{18}\text{O}_\text{P}$ variations. The high amount of precipitation falling in summer ($\sim 46\%$) should have a
400 strong effect and decrease the $\delta^{18}\text{O}_\text{P}$ values in the condensed water, while high temperatures
401 counteract this effect by increasing this ratio. Before reaching northeastern Canada, the air
402 masses pushed by the dominant westerly winds discharge most of their humidity over the land,

403 leading to a depleted $\delta^{18}\text{O}_\text{P}$ signal at our sites (for the same reason, $\delta^{18}\text{O}_\text{TR}$ values at L20, which is
404 located 110 km North-East of L01, are $\sim 1\text{‰}$ lower). Moreover, the $\delta^{18}\text{O}_\text{P}$ signal in the Canadian
405 sites is comparatively more depleted than in the Argentinian sites, because of their higher
406 latitude. It is worth noting that the resolution of the gridded meteorological dataset used for the
407 Canadian sites is relatively high (~ 10 km), which means that the local processes are likely well
408 represented.

409

410 **4.2. Relative performance in modelling $\delta^{18}\text{O}_\text{TR}$ values**

411 The simulated $\delta^{18}\text{O}_\text{TR}$ series based on daily $\delta^{18}\text{O}_\text{P}$ estimation from the regression models
412 reproduce the observations better than the ones based on $\delta^{18}\text{O}_\text{P}$ values derived from GCMs
413 (Figure 4). This is in part due to the greater number of parameters to optimize, as the calibration
414 process can more easily find a solution that fits the observations better. This may however reflect
415 error compensations especially in western Argentina where the estimated annual variability of
416 $\delta^{18}\text{O}_\text{P}$ is too large. Conversely in northeastern Canada, the annual variations of $\delta^{18}\text{O}_\text{P}$ that are
417 estimated, simulated by GCMs and observed are in good agreement (Figure SM2). Although
418 isotope-enabled atmospheric global models can reproduce the mean annual precipitation isotopic
419 values and seasonality for many areas (Risi et al., 2010), results at specific sites, especially in
420 mountainous regions such as at our western Argentinian site, can be less accurate (Figure SM2;
421 see the offset between GNIP stations and LMDZ-NCEP20). Ideally, daily $\delta^{18}\text{O}_\text{P}$ long-term
422 records from meteorological stations in the study region should be used as an input of
423 MAIDENiso. Simulations from high-resolution regional circulation models, such as REMOiso
424 which has a $0.5^\circ \times 0.5^\circ$ (~ 55 km) horizontal resolution (Insel et al., 2013; Sturm et al., 2007,
425 2005), may produce reliable local $\delta^{18}\text{O}_\text{P}$ values. Such dataset has proven to be quite helpful with
426 MAIDENiso in the Fontainebleau forest (France) (Danis et al., 2012). However, up to now,
427 measured or REMOiso $\delta^{18}\text{O}_\text{P}$ datasets in our regions of study do not exist, which is the case for
428 most regions of the world. Moreover, early data (1970-80s) from GNIP stations may have been
429 compromised by pan evaporation and therefore isotopic enrichment. Therefore, we recommend
430 that daily GNIP stations are set up in various forested ecosystems, that an effort is accomplished
431 to homogenize older GNIP time series, and that high resolution simulations of $\delta^{18}\text{O}_\text{P}$ are
432 performed in wider regions.

433

Aliénor Lavergne 9/10/y 14:14

Supprimé: en

435 The modelling of $\delta^{18}\text{O}_{\text{TR}}$ values based on the estimation of $\delta^{18}\text{O}_{\text{P}}$ is relatively more accurate for
436 northeastern Canada than for western Argentina (Figure 3). As the mean levels of the measured
437 $\delta^{18}\text{O}_{\text{TR}}$ values are high at the western Argentinian sites (mean value of about 30‰), the Bayesian
438 optimization tends to increase the biochemical (ϵ_0) and kinetic (ϵ_k) fractionations as well as the
439 coefficient a , while reducing the dampening factor (f_0) to reach more representative mean levels
440 of the $\delta^{18}\text{O}_{\text{TR}}$ simulation. But still, these levels are too low in comparison with the observations
441 (about 2.5‰ lower; Figure SM4). When the posterior value of a calibrated parameter is limited to
442 the upper bound of the prior range of plausible values, as it is the case at the western Argentinian
443 sites for a , b and ϵ_0 (Figure SM3), it means that either the prior range is too narrow, or the model
444 is inadequate, or some important process is not considered in the model. Here, the estimation of
445 the prior ranges of both coefficients a and b were based on observed (GNIP stations) and
446 simulated (GCMs) $\delta^{18}\text{O}_{\text{P}}$ values. Therefore, we expect their respective ranges to be consistent
447 with local processes. When the prior range of a is extended to higher values in the optimization
448 process, observed and simulated $\delta^{18}\text{O}_{\text{TR}}$ mean levels in western Argentina are better matching.
449 However, in this case, the distribution of $\delta^{18}\text{O}_{\text{P}}$ values is shifted toward higher values, advocating
450 for unrealistic estimated $\delta^{18}\text{O}_{\text{P}}$ variations.

451 One other possibility is that the prior range of ϵ_0 is too narrow. In accordance with DeNiro and
452 Epstein (1981), Sternberg (1989) and Yakir and DeNiro (1990), the biochemical fractionation ϵ_0
453 is assumed here to be lower than 30‰. However, a recent study has demonstrated that this
454 parameter, nearly constant between 20 to 30°C, increases at lower temperatures to values of 31‰
455 (Sternberg and Ellsworth, 2011). During the growing season, maximum temperatures can reach
456 20°C in western Argentina and 30°C in northeastern Canada, which suggests that the high mean
457 $\delta^{18}\text{O}_{\text{TR}}$ levels in *N. pumilio* may be due to biochemical fractionation higher than 30‰ due to
458 temperature generally lower than 20°C. However, when the prior range of ϵ_0 is extended to 31‰
459 in the optimization process, the mean $\delta^{18}\text{O}_{\text{TR}}$ levels of *N. pumilio* are still too low in comparison
460 with the observations. These results advocate for the existence of other processes, which can
461 explain this offset in mean levels in Argentina. For example, higher soil water evaporation than
462 modelled by MAIDENiso should lead to less negative $\delta^{18}\text{O}_{\text{SW}}$ (and therefore $\delta^{18}\text{O}_{\text{XW}}$), which
463 could explain the high mean levels of $\delta^{18}\text{O}_{\text{TR}}$ in Argentina. Caution should be exercised with such
464 an interpretation since other species living in similar conditions as *N. pumilio* in western
465 Argentina show comparatively lower mean $\delta^{18}\text{O}_{\text{TR}}$ levels than *N. pumilio* (i.e., *Fitzroya*

466 | *cupressoides*; see Lavergne et al., 2016). The ongoing monitoring and evaluation of isotopic
467 processes based on synchronous measurements of vapour, precipitation, soil water and xylem
468 water will certainly help understanding the high mean levels observed in Argentina, and
469 increasing the representation of the involved processes in MAIDENiso.

470

471 The better fit between observed and simulated $\delta^{18}\text{O}_{\text{TR}}$ values obtained with specific forms of
472 synthetic distributions of daily GPP for northeastern Canada and western Argentina (Figure 3)
473 suggests differential limiting factors in the two regions. The synthetic bimodal distribution of
474 daily GPP with maxima in spring and autumn, as simulated in western Argentina, is often
475 observed in a diversity of ecosystems such as in the Mediterranean environments (Baldocchi et
476 al., 2010; Gea-Izquierdo et al., 2015). After the activation of the photosynthesis in early spring,
477 increasing temperatures tend to be optimal for tree growth. However, in a modelling study,
478 Lavergne et al. (2015) have shown that the influence of temperature on *N. pumilio*'s growth
479 becomes negative once a temperature threshold (soil moisture) is exceeded. Therefore, we
480 assume that after reaching a threshold of temperature and soil moisture summer conditions, tree
481 growth is inhibited, leading to a decrease of primary productivity. However, when temperature
482 starts to decline and soil water supply tends to increase with increasing precipitation events, tree
483 growth increases again until the end of the growing season. In contrast, because precipitation is
484 more abundant in summer (June to September) in northeastern Canada (Naulier et al., 2014), high
485 summer temperatures should be always beneficial to tree growth if enough soil water is available.

486 Therefore, in agreement with GPP-derived eddy covariance data from the Fluxnet network (see
487 Gennaretti et al., 2017a), a better fit between observations and simulations is observed when
488 using a unimodal rather than a bimodal GPP distribution. Monitoring of tree physiology,
489 environmental conditions and wood cell formation will provide a more detailed representation of
490 the complex biological and ecological processes operating in Patagonia, allowing us to run the
491 MAIDENiso model with better constraints.

492

493 4.3. What is the main origin of the temperature signal recorded in $\delta^{18}\text{O}_{\text{TR}}$?

494 The investigation of the relative contributions of the isotopic composition of the source (xylem)
495 water and of the ^{18}O enrichment of the leaf water by transpiration on the simulated $\delta^{18}\text{O}_{\text{TR}}$ reveals
496 that the variability of the former has a weaker influence on $\delta^{18}\text{O}_{\text{TR}}$ variations than that of the

Aliénor Lavergne 9/10/y 14:14

Supprimé: . (

Aliénor Lavergne 9/10/y 14:14

Supprimé:).

Aliénor Lavergne 9/10/y 14:14

Supprimé: -

Aliénor Lavergne 9/10/y 14:14

Supprimé: . (

Aliénor Lavergne 9/10/y 14:14

Supprimé:).

502 latter in North and South America. Therefore, the temperature signal recorded in $\delta^{18}\text{O}_{\text{TR}}$ series
503 more likely reflects the effect of temperature on isotopic enrichment of the leaf water rather than
504 on the isotopic composition of the source water. At the leaf-level, air temperature has a strong
505 effect on the relative humidity and therefore on the vapour pressure deficit (VPD), i.e. the
506 difference between the saturation vapour pressure and the actual vapour pressure, which
507 modulates the transpiration (Barbour, 2007). Thus, the imprint of the ambient air temperature on
508 the fractionation processes occurring during transpiration is preferentially recorded in the tree
509 rings of the two species. Furthermore, both the isotopic signature of the xylem water and of the
510 fractionation processes occurring at the evaporation sites of the leaves have comparatively higher
511 influence on $\delta^{18}\text{O}_{\text{TR}}$ in *P. mariana* than in *N. pumilio*. This is probably due to the lower amplitude
512 of the day-by-day variations of the relative humidity in western Argentina (SD = 5%) versus in
513 northeastern Canada (SD = 16%) that translates into a weaker influence of h_{air} variations and
514 therefore of leaf-level isotopic fractionation processes on $\delta^{18}\text{O}_{\text{TR}}$ values in western Argentina
515 than in northeastern Canada. These results highlight the potential of MAIDENiso model to better
516 refine the origin of the climatic signal recorded in the oxygen isotopic signature in the tree rings
517 of different species.

518

519 5. CONCLUSION

520 Here, by using MAIDENiso model, we have provided a mechanistic overview of the climatic and
521 biological processes controlling oxygen isotopic fractionation in two American temperature-
522 sensitive tree species. First, we have shown that using regression-based rather than model-based
523 $\delta^{18}\text{O}_{\text{P}}$ estimates as inputs increases the predictive skills of our simulations, although this may be
524 at the price of error compensations. Second, our study reveals that the variability of the isotopic
525 composition of the source (xylem) water has a weaker influence on $\delta^{18}\text{O}_{\text{TR}}$ variations than that of
526 the ^{18}O enrichment of the leaf water by transpiration. Last, these findings suggest that the imprint
527 of temperature recorded in $\delta^{18}\text{O}_{\text{TR}}$ of the two species is likely related to the effect of temperature
528 on isotopic enrichment of the leaf water. The isotopic monitoring of water within the soil-
529 vegetation-atmosphere compartments in future work will certainly provide the input and control
530 data necessary to better constrain MAIDENiso. Our study demonstrates that the eco-
531 physiological modelling of $\delta^{18}\text{O}_{\text{TR}}$ values is necessary and likely the only approach to accurately
532 interpret the recorded climate signal. Based on the calibrations of MAIDENiso presented here,

Aliénor Lavergne 9/10/y 14:14

Supprimé: -

534 the next step involves inverse modelling approaches to perform paleoclimatic reconstructions in
535 North and South America that are less biased by the complex and nonlinear interactions between
536 climate, CO₂ concentrations and tree growth as recommended by Boucher et al. (2014).

537

538 **Code and data availability**

539 The code of the model can be found in <https://doi.org/10.6084/m9.figshare.5446435.v1>. The daily
540 $\delta^{18}\text{O}_\text{p}$ data from the MUGCM model were extracted via the SWING project webpage
541 (<http://paos.colorado.edu/~dcn/SWING/database.php>). The daily climatic data used for Quebec
542 were retrieved from <http://cfs.nrcan.gc.ca/projects/3/4>, while those for Argentina were extracted
543 from https://www.esrl.noaa.gov/psd/data/gridded/data.20thC_ReanV2c.html. The atmospheric
544 CO₂ concentration data derived from the Mauna Loa station were extracted from
545 <http://www.esrl.noaa.gov/gmd/ccgg/trends/>.

546

547 **ACKNOWLEDGMENTS**

548 A.L. has been supported by a Research associate/Lecturer position at the Aix-Marseille
549 University (France). F.G. has received funding from the European Union's Horizon 2020
550 research and innovation program under the Marie Skłodowska-Curie grant agreement No
551 656896. We acknowledge all data providers: the Instituto Argentino de Nivología, Glaciología y
552 Ciencias Ambientales (IANIGLA, Argentina) for providing the daily temperature data from La
553 Almohadilla site; the National Meteorological Service from Argentina for providing the monthly
554 temperature data from Bariloche meteorological station (Argentina); the Department of Natural
555 Resources Canada for providing the daily climatic data used for Quebec; the US Department of
556 Energy, Office of Science Biological and Environmental Research (BER) and the National
557 Oceanic and Atmospheric Administration Climate Program Office for providing the daily
558 climatic data used for Argentina; and the SWING project for providing the daily $\delta^{18}\text{O}_\text{p}$ data from
559 MUGCM model.

560

561

References

562 Baldocchi, D. D., Ma, S., Rambal, S., Misson, L., Ourcival, J. M., Limousin, J. M., Pereira, J. and
563 Papale, D.: On the differential advantages of evergreenness and deciduousness in mediterranean
564 oak woodlands: A flux perspective, *Ecol. Appl.*, 20(6), 1583–1597, doi:10.1890/08-2047.1, 2010.

565 Barbour, M. M.: Stable oxygen isotope composition of plant tissue: a review, *Funct. Plant Biol.*,
 566 34, 83–94, doi:10.1071/FP06228, 2007.

567 Barbour, M. M., Cernusak, L. A. and Farquhar, G. D.: Factors affecting the oxygen isotope ratio
 568 of plant organic material, in *Stable isotopes and biosphere-atmosphere interactions: Processes*
 569 *and Biological Controls*, edited by L. B. Flanagan, J. R. Ehleringer, and D. E. Pataki, pp. 9–28,
 570 Elsevier, Amsterdam., 2005.

571 Boucher, E., Guiot, J., Hatté, C., Daux, V., Danis, P. A. and Dussouillez, P.: An inverse modeling
 572 approach for tree-ring-based climate reconstructions under changing atmospheric CO₂
 573 concentrations, *Biogeosciences*, 11(12), 3245–3258, 2014.

574 Brienien, R. J. W., Helle, G., Pons, T. L., Guyot, J.-L. and Gloor, M.: Oxygen isotopes in tree
 575 rings are a good proxy for Amazon precipitation and El Niño-Southern Oscillation variability,
 576 *Proc. Natl. Acad. Sci.*, 109(42), 16957–16962, doi:10.1073/pnas.1205977109, 2012.

577 Buhay, W. M., Edwards, T. W. D. and Aravena, R.: Evaluating kinetic fractionation factors used
 578 for reconstructions from oxygen and hydrogen isotope ratios in plant water and cellulose,
 579 *Geochemistry, Geophys. Geosystems*, 60(12), 2209–2218, 1996.

580 Cernusak, L. A. and English, N. B.: Beyond tree-ring widths: stable isotopes sharpen the focus on
 581 climate responses of temperate forest trees, *Tree Physiol.*, 35(1), 1–3,
 582 doi:10.1093/treephys/tpu115, 2015.

583 Compo, G. P., Whitaker, J. S., Sardeshmukh, P. D., Matsui, N., Allan, R. J., Yin, X., Gleason, B.
 584 E., Vose, R. S., Rutledge, G., Bessemoulin, P., BroNnimann, S., Brunet, M., Crouthamel, R. I.,
 585 Grant, A. N., Groisman, P. Y., Jones, P. D., Kruk, M. C., Kruger, A. C., Marshall, G. J., Maugeri,
 586 M., Mok, H. Y., Nordli, O., Ross, T. F., Trigo, R. M., Wang, X. L., Woodruff, S. D. and Worley,
 587 S. J.: The twentieth century reanalysis project, *Q. J. R. Meteorol. Soc.*, 137(654), 1–28,
 588 doi:10.1002/qj.776, 2011.

589 Craig, H. and Gordon, L. I.: Deuterium and oxygen 18 variations in the ocean and the marine
 590 atmosphere, Spoleto, 1965.

591 Danis, P. A., Hatté, C., Misson, L. and Guiot, J.: MAIDENiso: a multiproxy biophysical model of
 592 tree-ring width and oxygen and carbon isotopes, *Can. J. For. Res.*, 42(9), 1697–1713,
 593 doi:10.1139/x2012-089, 2012.

594 Danis, P. A., Masson-Delmotte, V., Stievenard, M., Guillemin, M. T., Daux, V., Naveau, P. and
 595 von Grafenstein, U.: Reconstruction of past precipitation $\delta^{18}\text{O}$ using tree-ring cellulose $\delta^{18}\text{O}$ and

596 $\delta^{13}\text{C}$: A calibration study near Lac d'Annecy, France, *Earth Planet. Sci. Lett.*, 243(3–4), 439–448,
597 doi:10.1016/j.epsl.2006.01.023, 2006.

598 Dansgaard, W.: Stable isotopes in precipitation, *Tellus A*, 16(4), 436–468,
599 doi:10.3402/tellusa.v16i4.8993, 1964.

600 DeNiro, M. J. and Epstein, S.: Relationship between the oxygen isotope ratios of terrestrial plant
601 cellulose, carbon dioxide, and water, *Science*, 204, 51–53, 1979.

602 DeNiro, M. J. and Epstein, S.: Isotopic composition of cellulose from aquatic organisms,
603 *Geochim. Cosmochim. Acta*, 45(10), 1885–1894, doi:10.1016/0016-7037(81)90018-1, 1981.

604 Donoso, C.: Tipos forestales de los bosques nativos de Chile., Documento de Trabajo Nu. 38.
605 Investigación y Desarrollo Forestal (CONAF, PNUD-FAO). FAO Chile., 1981.

606 Farquhar, G. D., Barbour, M. M. and Henry, B. K.: Interpretation of oxygen isotope composition
607 of leaf material, in *Stable isotopes: integration of biological, ecological and geochemical*
608 *processes*, pp. 27–61, BIOS Scientific Publishers: Oxford., 1998.

609 Farquhar, G. D., Hubick, H. T., Condon, A. G. and Richards, R. A.: Carbon isotope fractionation
610 and plant water-use efficiency, in *Stable isotopes in ecological research*, pp. 21–40., 1989.

611 Gea-Izquierdo, G., Guibal, F., Joffre, R., Ourcival, J. M., Simioni, G. and Guiot, J.: Modelling
612 the climatic drivers determining photosynthesis and carbon allocation in evergreen Mediterranean
613 forests using multiproxy long time series, *Biogeosciences*, 12(12), 3695–3712, doi:10.5194/bg-
614 12-3695-2015, 2015.

615 Gennaretti, F., Arseneault, D., Nicault, A., Perreault, L. and Bégin, Y.: Volcano-induced regime
616 shifts in millennial tree-ring chronologies from northeastern North America., *Proc. Natl. Acad.*
617 *Sci. U. S. A.*, 111(28), 10077–10082, doi:10.1073/pnas.1324220111, 2014.

618 Gennaretti, F., Gea-Izquierdo, G., Boucher, E., Berninger, F., Arseneault, D. and Guiot, J.:
619 Ecophysiological modeling of the climate imprint on photosynthesis and carbon allocation to the
620 tree stem in the North American boreal forest, *Biogeosciences Discuss.*, in review,
621 doi:10.5194/bg-2017-51, 2017a.

622 Gennaretti, F., Huard, D., Naulier, M., Savard, M., Bégin, C., Arseneault, D. and Guiot, J.:
623 Bayesian multiproxy temperature reconstruction with black spruce ring widths and stable
624 isotopes from the northern Quebec taiga, *Clim. Dyn.*, 1–13, doi:10.1007/s00382-017-3565-5,
625 2017b.

626 Gessler, A., Ferrio, J. P., Hommel, R., Treydte, K., Werner, R. A. and Monson, R. K.: Stable

isotopes in tree rings: towards a mechanistic understanding of isotope fractionation and mixing processes from the leaves to the wood., *Tree Physiol.*, 0, 1–23, 2014.

Guiot, J., Boucher, E. and Gea-Izquierdo, G.: Process models and model-data fusion in dendroecology, *Front. Ecol. Evol.*, 2, 52, doi:10.3389/fevo.2014.00052, 2014.

Hartl-Meier, C., Zang, C., Büntgen, U. L. F., Esper, J. A. N., Rothe, A., Göttelein, A., Dirnböck, T. and Treydte, K.: Uniform climate sensitivity in tree-ring stable isotopes across species and sites in a mid-latitude temperate forest., *Tree Physiol.*, 2003(1), 4–15, doi:10.1093/treephys/tpu096, 2014.

Helliker, B. R. and Richter, S. L.: Subtropical to boreal convergence of tree-leaf temperatures, *Nature*, 454(7203), 511–514, doi:10.1038/nature07031, 2008.

Horita, J. and Wesolowski, D. J.: Liquid-vapor fractionation of oxygen and hydrogen isotopes of water from the freezing to the critical temperature, *Geochim. Cosmochim. Acta*, 58(16), 3425–3437, doi:10.1016/0016-7037(94)90096-5, 1994.

Hourdin, F., Grandpeix, J. Y., Rio, C., Bony, S., Jam, A., Cheruy, F., Rochetin, N., Fairhead, L., Idelkadi, A., Musat, I., Dufresne, J. L., Lahellec, A., Lefebvre, M. P. and Roehrig, R.: LMDZ5B: The atmospheric component of the IPSL climate model with revisited parameterizations for clouds and convection, *Clim. Dyn.*, 40(9–10), 2193–2222, doi:10.1007/s00382-012-1343-y, 2013.

Hutchinson, M. F., McKenney, D. W., Lawrence, K., Pedlar, J. H., Hopkinson, R. F., Milewska, E. and Papadopol, P.: Development and testing of Canada-wide interpolated spatial models of daily minimum-maximum temperature and precipitation for 1961-2003, *J. Appl. Meteorol. Climatol.*, 48(4), 725–741, doi:10.1175/2008JAMC1979.1, 2009.

Insel, N., Poulsen, C. J., Sturm, C. and Ehlers, T. A.: Climate controls on Andean precipitation $\delta^{18}\text{O}$ interannual variability, *J. Geophys. Res. Atmos.*, 118(17), 9721–9742, doi:10.1002/jgrd.50619, 2013.

Kahmen, A., Sachse, D., Arndt, S. K., Tu, K. P., Farrington, H., Vitousek, P. M. and Dawson, T. E.: Cellulose $\delta^{18}\text{O}$ is an index of leaf-to-air vapor pressure difference (VPD) in tropical plants., *Proc. Natl. Acad. Sci. U. S. A.*, 108(5), 1981–1986, doi:10.1073/pnas.1018906108, 2011.

Keeling, C. D., Bacastow, R. B., Bainbridge, A. E., Ekdahl Jr., C. A., Guenther, P. R., Waterman, L. S. and Chin, J. F. S.: Atmospheric carbon dioxide variations at Mauna Loa Observatory, Hawaii, *Tellus A*, 28, 538–551, doi:10.3402/tellusa.v28i6.11322, 1976.

658 Labuhn, I., Daux, V., Girardclos, O., Stievenard, M., Pierre, M. and Masson-Delmotte, V.:
 659 French summer droughts since 1326 AD: a reconstruction based on tree ring cellulose $\delta^{18}\text{O}$,
 660 Clim. Past, 11(6), 5113–5155, doi:10.5194/cpd-11-5113-2015, 2016.
 661 Lavergne, A., Daux, V., Villalba, R. and Barichivich, J.: Temporal changes in climatic limitation
 662 of tree-growth at upper treeline forests: Contrasted responses along the west-to-east humidity
 663 gradient in Northern Patagonia, Dendrochronologia, 36, 49–59, 2015.
 664 Lavergne, A., Daux, V., Villalba, R., Pierre, M., Stievenard, M. and Srur, A. M.: Improvement of
 665 isotope-based climate reconstructions in Patagonia through a better understanding of climate
 666 influences on isotopic fractionation in tree rings, Earth Planet. Sci. Lett., 459, 372–380,
 667 doi:10.1016/j.epsl.2016.11.045, 2017.
 668 Lavergne, A., Daux, V., Villalba, R., Pierre, M., Stievenard, M., Srur, A. M. and Vimeux, F.: Are
 669 the $\delta^{18}\text{O}$ of *F. cupressoides* and *N. pumilio* promising proxies for climate reconstructions in
 670 northern Patagonia?, J. Geophys. Res. - Biogeosciences, 121(3), 767–776,
 671 doi:10.1002/2015JG003260, 2016.
 672 López Bernal, P., Defossé, G. E., Quinteros, C. P. and Bava, J. O.: Sustainable management of
 673 lenga (*Nothofagus pumilio*) forests through group selection system, in Sustainable forest
 674 management - current research, edited by D. J. J. D. (Ed.), pp. 45–66, 2012.
 675 Lorrey, A. M., Brookman, T. H., Evans, M. N., Fauchereau, N.C., Barbour, M., Macinnis-Ng, C.
 676 Criscitiello, A., Eischeid, G., Fowler, A. M., Horton, T. W. and Schrag, D. P.: Stable oxygen
 677 isotope signatures of early season wood in New Zealand kauri (*Agathis australis*) tree rings:
 678 Prospects for palaeoclimate reconstruction., Dendrochronologia, 40, 50–63, doi:
 679 10.1016/j.dendro.2016.03.012, 2016.
 680 Magnin, A., Puntieri, J. and Villalba, R.: Interannual variations in primary and secondary growth
 681 of *Nothofagus pumilio* and their relationships with climate, Trees, 28(5), 1463–1471, 2014.
 682 Misson, L.: MAIDEN: a model for analyzing ecosystem processes in dendroecology, Can. J. For.
 683 Res., 34, 874–887, 2004.
 684 Naulier, M., Savard, M. M., Bégin, C., Gennaretti, F., Arseneault, D., Marion, J., Nicault, A. and
 685 Bégin, Y.: A millennial summer temperature reconstruction for northeastern Canada using
 686 oxygen isotopes in subfossil trees, Clim. Past, 11(9), 1153–1164, doi:10.5194/cp-11-1153-2015,
 687 2015.
 688 Naulier, M., Savard, M. M., Bégin, C., Marion, J., Arseneault, D. and Bégin, Y.: Carbon and

689 oxygen isotopes of lakeshore black spruce trees in northeastern Canada as proxies for climatic
 690 reconstruction, *Chem. Geol.*, 374–375, 37–43, doi:10.1016/j.chemgeo.2014.02.031, 2014.
 691 Noone, D. and Simmonds, I.: Associations between $\delta^{18}\text{O}$ of water and climate parameters in a
 692 simulation of atmospheric circulation for 1979–95, *J. Clim.*, 15, 3150–3169, 2002.
 693 Ogée, J., Barbour, M. M., Wingate, L., Bert, D., Bosc, A., Stievenard, M., Lambrot, C., Pierre,
 694 M., Bariac, T., Loustau, D. and Dewar, R. C.: A single-substrate model to interpret intra-annual
 695 stable isotope signals in tree-ring cellulose, *Plant, Cell Environ.*, 32(8), 1071–1090,
 696 doi:10.1111/j.1365-3040.2009.01989.x, 2009.
 697 Ogée, J., Brunet, Y., Loustau, D., Berbigier, P. and Delzon, S.: MuSICA, a CO_2 , water and
 698 energy multilayer, multileaf pine forest model: Evaluation from hourly to yearly time scales and
 699 sensitivity analysis, *Glob. Chang. Biol.*, 9(5), 697–717, doi:10.1046/j.1365-2486.2003.00628.x,
 700 2003.
 701 Rinne, K. T., Loader, N. J., Switsur, V. R. and Waterhouse, J. S.: 400-year May-August
 702 precipitation reconstruction for Southern England using oxygen isotopes in tree rings, *Quat. Sci.*
 703 *Rev.*, 60, 13–25, doi:10.1016/j.quascirev.2012.10.048, 2013.
 704 Risi, C., Bony, S., Vimeux, F. and Jouzel, J.: Water-stable isotopes in the LMDZ4 general
 705 circulation model: Model evaluation for present-day and past climates and applications to
 706 climatic interpretations of tropical isotopic records, *J. Geophys. Res. Atmos.*, 115(12), 1–27,
 707 doi:10.1029/2009JD013255, 2010.
 708 Roden, J. S., Lin, G. and Ehleringer, J. R.: A mechanistic model for interpretation of hydrogen
 709 and oxygen isotope ratios in tree-ring cellulose, *Geochim. Cosmochim. Acta*, 64(1), 21–35,
 710 doi:10.1016/S0016-7037(99)00195-7, 2000.
 711 Rozanski, K., Araguás-Araguás, L.: Spatial and temporal variability of stable isotope
 712 composition of precipitation over the South American continent, *Bull. l’Institut Fr. d’études*
 713 *Andin.*, 24(3), 379–390, 1995.
 714 Rozanski, K., Araguás-Araguás, L. and Gonfiantini, R.: Isotopic patterns in modern global
 715 precipitation, in *Climate change in continental isotopic records.*, edited by P. K. Swart, K. C.
 716 Lohmann, J. McKenzie, and S. Savin, American Geophysical Union., 1993.
 717 Running, S. W., Nemani, R. R. and Hungerford, R. D.: Extrapolation of synoptic meteorological
 718 data in mountainous terrain and its use for simulating forest evapotranspiration and
 719 photosynthesis, *Can. J. For. Res.*, 17, 472–483, doi:10.1139/x87-081, 1987.

720 Rusch, V. E.: Altitudinal variation in the phenology of *Nothofagus pumilio* in Argentina, *Rev.*
 721 *Chil. Hist. Nat.*, 66(2), 131–141, 1993.
 722 Saurer, M., Aellen, K. and Siegwolf, R. T. W.: Correlating $\delta^{13}\text{C}$ and $\delta^{18}\text{O}$ in cellulose of trees,
 723 *Plant, Cell Environ.*, 20, 1543–1550, 1997.
 724 Saurer, M., Cherubini, P., Reynolds-Henne, C. E., Treydte, K. S., Anderson, W. T. and Siegwolf,
 725 R. T. W.: An investigation of the common signal in tree ring stable isotope chronologies at
 726 temperate sites, *J. Geophys. Res. Biogeosciences*, 113(4), doi:10.1029/2008JG000689, 2008.
 727 Schlatter, J.: Requerimientos de sitio para la lenga, *Nothofagus pumilio* (Poepp. et Endl.) Krasser,
 728 *Bosque*, 15, 3–10, 1994.
 729 Shi, C., Daux, V., Zhang, Q. B., Risi, C., Hou, S. G., Stievenard, M., Pierre, M., Li, Z. and
 730 Masson-Delmotte, V.: Reconstruction of southeast Tibetan Plateau summer climate using tree
 731 ring $\delta^{18}\text{O}$: Moisture variability over the past two centuries, *Clim. Past*, 8(1), 205–213,
 732 doi:10.5194/cp-8-205-2012, 2012.
 733 Smith, R. B. and Evans, J. P.: Orographic precipitation and water vapor fractionation over the
 734 Southern Andes, *J. Hydrometeorol.*, 8(1), 3–19, doi:10.1175/JHM555.1, 2007.
 735 Stern, L. A. and Blisniuk, P. M.: Stable isotope composition of precipitation across the southern
 736 Patagonian Andes, *J. Geophys. Res. Atmos.*, 107(23), doi:10.1029/2002JD002509p, 2002.
 737 Sternberg, L. D. S. L.: Oxygen and hydrogen isotope ratios in plant cellulose: Mechanisms and
 738 applications, in *Stable isotopes in ecological research*, edited by J. R. E. and K. A. N. P. W.
 739 Rundel, pp. 124–141., 1989.
 740 Sternberg, L. D. S. L. and Ellsworth, P. F. V.: Divergent biochemical fractionation, not
 741 convergent temperature, explains cellulose oxygen isotope enrichment across latitudes, *PLoS*
 742 *One*, 6(11), e28040, doi:10.1371/journal.pone.0028040, 2011.
 743 Sturm, C., Vimeux, F. and Krinner, G.: Intraseasonal variability in South America recorded in
 744 stable water isotopes, *J. Geophys. Res. Atmos.*, 112(20), doi:10.1029/2006JD008298, 2007.
 745 Sturm, K., Hoffmann, G., Langmann, B. and Stichler, W.: Simulation of $\delta^{18}\text{O}$ in precipitation by
 746 the regional circulation model REMOiso, *Hydrol. Process.*, 19(17), 3425–3444,
 747 doi:10.1002/hyp.5979, 2005.
 748 Treydte, K., Boda, S., Graf Pannatier, E., Fonti, P., Frank, D., Ullrich, B., Saurer, M., Siegwolf,
 749 R. T. W., Battipaglia, G., Werner, W. and Gessler, A.: Seasonal transfer of oxygen isotopes from
 750 precipitation and soil to the tree ring: Source water versus needle water enrichment, *New Phytol.*,

751 202(3), 772–783, doi:10.1111/nph.12741, 2014.
752 Viereck, L. A. and Johnston, W. F.: *Picea mariana* (Mill.) B. S. P., in *Silvics of North America*:
753 1. Conifers; 2. Hardwoods., edited by R. M. Burns and B. H. Honkala, pp. 443–464, US.
754 Department of Agriculture, Forest Service, Washington, DC., 1990.
755 Wernicke, J., Griebinger, J., Hochreuther, P. and Brauning, A.: Variability of summer humidity
756 during the past 800 years on the eastern Tibetan Plateau inferred from $\delta^{18}\text{O}$ of tree-ring cellulose.,
757 *Clim. Past*, 11, 327–337, doi:10.5194/cp-11-327-2015, 2015.
758 Wershaw, R. L., Friedman, I. and Heller, S. J.: Hydrogen isotope fractionation in water passing
759 through trees, in *Advances in Organic Geochemistry*, edited by F. Hobson and M. Speers, pp. 55–
760 67, New York, Pergamon., 1966.
761 Yakir, D. and DeNiro, M. J.: Oxygen and hydrogen isotope fractionation during cellulose
762 metabolism in *lemna gibba* L., *Plant Physiol.*, 93(1), 325–332, doi:10.1104/pp.93.1.325, 1990.
763
764 |

Tables and Figures

Table 1 Definition of sensitive parameters. The posterior medians and 90% confidence intervals are also shown.

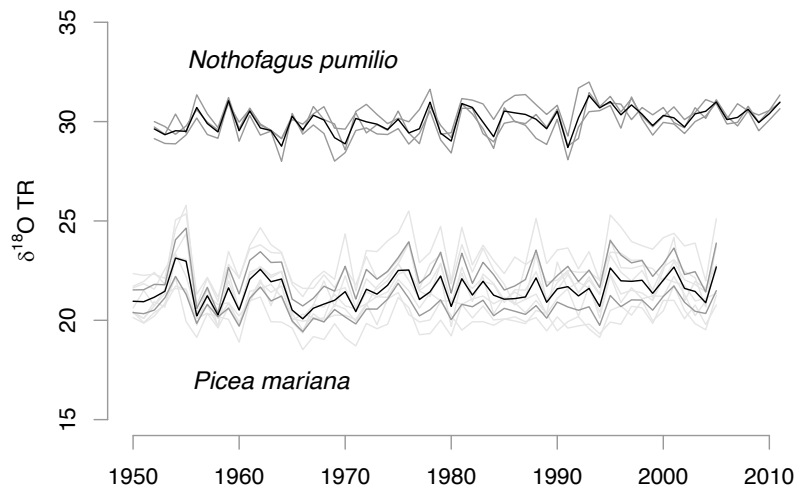
Parameter	Definition	Unit	Parameter type (prior range)	Values with 90% posterior confidence intervals
f_0	Dampening factor	NA	Calibrated (0.3 to 0.5)	0.36 [0.31; 0.46] (Arg.) 0.41 [0.32; 0.48] (Q.)
ϵ_0	Biochemical fractionation	‰	Calibrated (24 to 30)	29.99 [29.93; 30] (Arg.) 26.81 [24.74; 28.04] (Q.)
ϵ_k	Kinetic fractionation	‰	Calibrated (10 to 30)	28.86 [18.25; 29.96] (Arg.) 17.20 [11.16; 26.34] (Q.)
a	Temperature dependence of $\delta^{18}\text{O}_p$	NA	Calibrated (0.2 to 0.5 for Arg. and 0 to 0.38 for Q.)	0.50 [0.49; 0.50] (Arg.) 0.31 [0.25; 0.37] (Q.)
b	Precipitation dependence of $\delta^{18}\text{O}_p$	NA	Calibrated (-0.3 to 0 for Arg. and -0.39 to 0 for Q.)	-0.009 [-0.15; 0] (Arg.) -0.22 [-0.35; -0.14] (Q.)
c	Intercept of $\delta^{18}\text{O}_p$	‰	Fixed	-10.0 (Arg.) -11.9 (Q.)

774 **Table 2** Climate input data for all tested simulations
775

	Daily Tmin and Tmax	Daily P	Daily $\delta^{18}\text{O}_\text{p}$	CO ₂
Configuration 1	Canadian database/ NOAA-CIRES dataset		Linear regression	Mauna Loa station
Configuration 2	Canadian database / NOAA-CIRES dataset	MUGCM data		
Configuration 3	LMDZ-NCEP20 data			

776
777

778 | **Figure 1** Tree ring $\delta^{18}\text{O}$ time series (‰) at the three sites in Argentina (NUB, ALM and CHA in
779 | dark grey) and two sites in Quebec (L01 and L20 in dark grey; single trees in light grey). The
780 | bold black lines are the averaged values. The mean inter-site correlation coefficients are
781 | $r = 0.60$, $p < 0.05$ and $r = 0.80$, $p < 0.01$ in the South and North American sites, respectively.

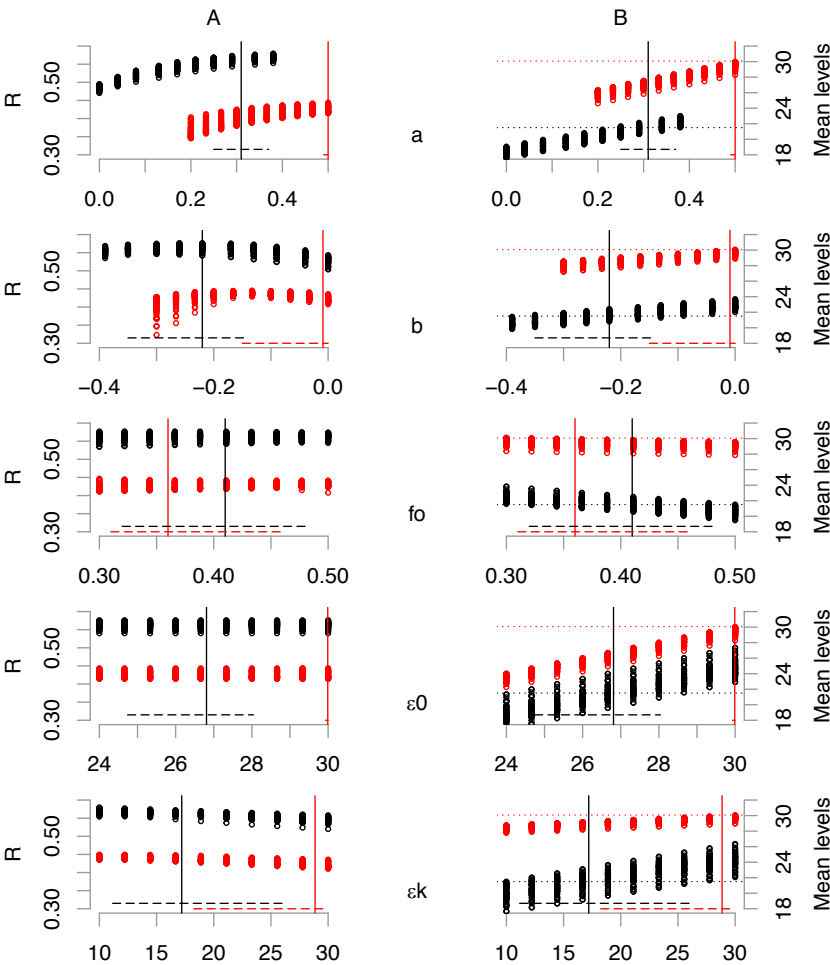


Aliénor Lavergne 9/10/y 14:14
Supprimé: -

Aliénor Lavergne 9/10/y 14:14
Supprimé: 01in

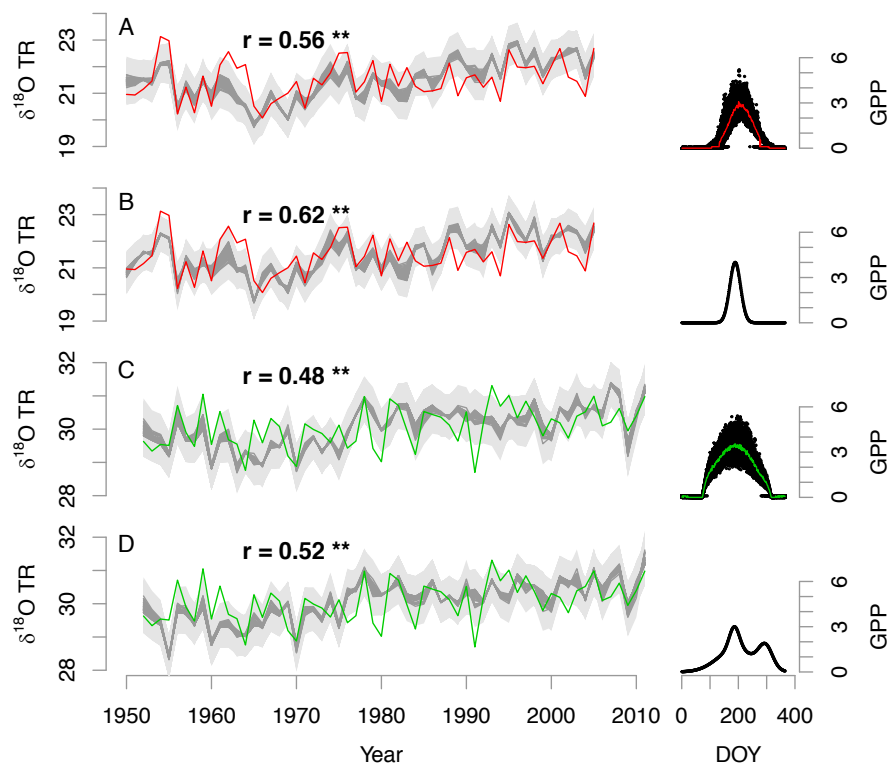
783
784

787 **Figure 2** Dependence of the correlation coefficients between observed and simulated $\delta^{18}\text{O}_{\text{TR}}$
 788 series (panels A), and of the mean simulated $\delta^{18}\text{O}_{\text{TR}}$ levels (‰) (panels B) as a function of the
 789 range of calibrated parameters a , b , f_o , ε_0 and ε_k for the 50 simulations performed. The tests sites
 790 from Quebec are in black and the Argentinean ones are in red. The vertical lines are the values of
 791 a plausible block of parameters retained in the MCMC optimization. The horizontal dashed lines
 792 are their respective 90% confidence interval calculated with 50 simulations (see Table 1). The
 793 horizontal dot lines in panel B are the mean values of the observed $\delta^{18}\text{O}_{\text{TR}}$.



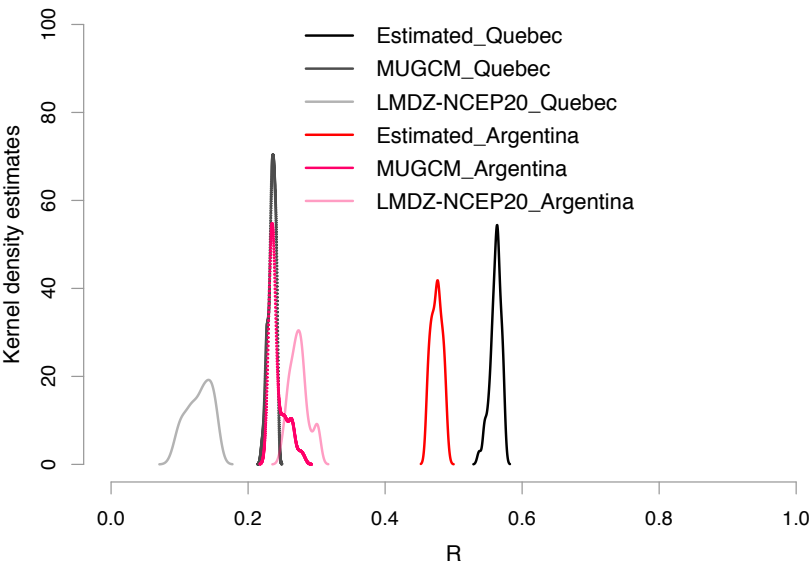
Aliénor Lavergne 9/10/y 14:14
 Supprimé: In black are the
 Aliénor Lavergne 9/10/y 14:14
 Supprimé: with the
 Aliénor Lavergne 9/10/y 14:14
 Mis en forme: Français
 Aliénor Lavergne 9/10/y 14:14
 Mis en forme: Français
 Aliénor Lavergne 9/10/y 14:14
 Supprimé: sites
 Aliénor Lavergne 9/10/y 14:14
 Mis en forme: Français
 Aliénor Lavergne 9/10/y 14:14
 Supprimé: in red the oneswith
 Aliénor Lavergne 9/10/y 14:14
 Mis en forme: Français

799 **Figure 3** Comparison between observed (red or green) and simulated (grey) $\delta^{18}\text{O}_{\text{TR}}$ chronologies
800 in Quebec (A and B) and Argentina (C and D), respectively, using GPP (in $\text{gC.m}^{-2}.\text{day}^{-1}$)
801 simulated by MAIDENiso for each day of the year (DOY) (A and C) or synthesized for
802 maximizing correlations (B and D). The simulations are based on estimated $\delta^{18}\text{O}_{\text{P}}$ series. The 50
803 different simulations inferred from the Markov Chain Monte Carlo (MCMC) chains are in dark grey.
804 The ± 1 root mean square error (RMSE) range is represented in light grey. The mean
805 correlation coefficients are significant at 99% level (**).



806
807

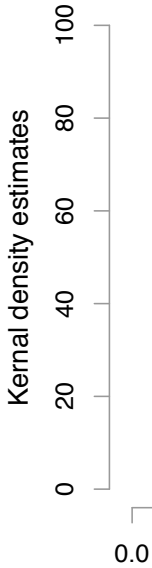
808 | **Figure 4** Density distributions of the coefficient of correlation (R) between observed and
809 simulated $\delta^{18}\text{O}_{\text{TR}}$ chronologies in Quebec and Argentina when the simulations are based on $\delta^{18}\text{O}_{\text{p}}$
810 series estimated by the regression model or from the MUGCM and LMDZ-NCEP20 models.
811



Aliénor Lavergne 9/10/y 14:14

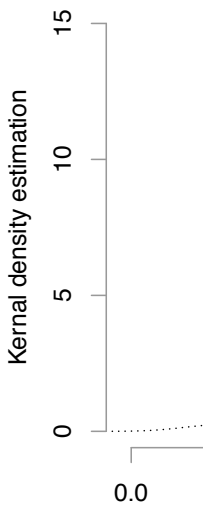
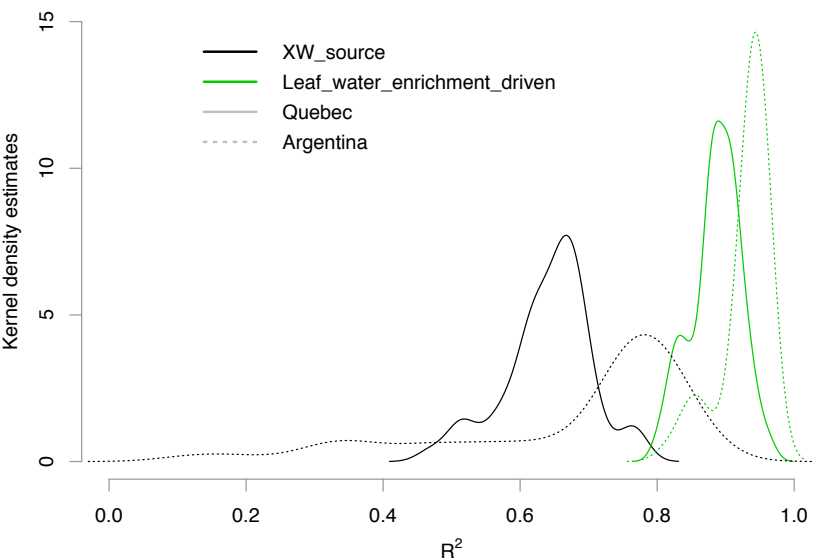
Supprimé: Comparison of the densities of probability

Aliénor Lavergne 9/10/y 14:14



Supprimé:

817 **Figure 5** Density distributions of the coefficients of determination (R^2) between the reference
818 simulations and the: 1) XW source experiment simulation ($\delta^{18}\text{O}_v$ and h_{air} set as constant, black)
819 and, 2) Leaf water enrichment driven experiment simulation ($\delta^{18}\text{O}_{\text{XW}}$ set as constant, green) in
820 Quebec (bold line) and Argentina (dashed line).



Aliénor Lavergne 9/10/y 14:14

Supprimé:

... [1]